https://dx.doi.org/10.22161/ijaers.74.18 ISSN: 2349-6495(P) | 2456-1908(O)

Preparation of PANI Nanorods on C-ZIF-8 Seed Layer by UPED Method as Ultra-thin Elastic Electrode for Flexible Capacitor

Ayman Alameen[1], Huixin Zhang[1], Tongtong Jin[2], Xiaofan Fang[2], Xiao DU[1], Xuli Ma[2]

[1]Department of Chemical Engineering, Taiyuan University of Technology, Taiyuan 030024, China
[2]Department of Environmental Science and Engineering, Taiyuan University of Technology, Taiyuan 030024, China

Abstract**—** *Novel ultra-thin PANI nanorods were growth on the aspheric-shape C-ZIF-8 seed layer coated stainless steel wire mesh (SSWM) flexible substrate as an elastic electrode for the flexible capacitor. Synthesized by Unipolar Pulse Electrodeposition (UPED) method, the unique ultra-thin thickness of C-ZIF/PANI nanorods electrode (10 - 20 µm) were capable of withstanding under critical flexes situation, due to losing the flexion strength as convergence or divergence between the aspheric-shape C-ZIF-8 particles. The morphology growth of PANI nanorods was significantly dependent on the anilinium micellar transformation, relatively long relaxation period (off-time), and the electrodeposit time and cycles numbers. UPED electrodeposition strategy preform to control the electrodeposition cycles and time. BET surface measurement, scanning electron microscopy SEM, X-ray diffraction, and FTIR spectra were measured to characterize the surface morphology of the elastic electrode. Besides, the phenomena role of UPED method in the fabrication process were discussed.*

Keywords**— PANI nanorods, C-ZIF-8/PANI composite, UPED Electrodeposition, flexible supercapacitor.**

I. INTRODUCTION

To satisfying the fast-growing of the portable and wearable electronics market, simultaneously avoid the environmental pollution caused by the consumption of fossil fuels, as a widely used energy source, demand to develop environmentally-friendly flexible energy storage devices, with high energy and power density [1]. Supercapacitors (SCs) bridge the gaps between batteries and conventional capacitors in terms of the energy-power density [2], nowadays flexible capacitor is the strong candidate capable of bridging the gap in the portable and wearable application, in the term of flexible energy storage device, with the stable electrochemical performance [3-6]. But enormous drawback in the capacitance of the flexible capacitor occurs when flexion the electrochemical circuit or device, hindering the efficient applicable of the flexible SCs in the energy storage field [7], This primarily attributed to disintegrating the electrode materials effected by flexion the flexible supercapacitor circuit. Herein the research gaps motivate us to investigate the question of how to develop elastic electrode material capable to harmonically flexion compatible with the flexible substrate flexion? in order to avoid the obstacle of fragmentize the electrode active material, simultaneously maintain the same devise efficiency under the different flexion situation.

Carbon materials, metal oxides, and conducting polymers are the most reported appropriate electrode materials, due to the excellent electrochemical properties of those materials [8,9]. Meanwhile, the composite of those materials combines the individual characteristics of each material in the final produced composite, resulting in enhance the adequacy of the general electrochemical circuit [10]. Whoever the intrinsic aggregation of the particles constructing the whole composite is rigid, and applying any flexion strength to manipulate the electrochemical circuit, can quickly disintegrate the electrode surface-active materials [11], leading to a sharp decline in the overall gravimetric capacitance of the flexible capacitor [12]. Our previous work Flexible All-Solid-State Supercapacitor Based on Polyhedron C-ZIF-8/PANI Composite Synthesized by Unipolar Pulse Electrodeposition Method (UPED), demonstrate the capability of C-ZIF-8/PANI composite to stabilize the capacitance of the flexible capacitor devises, in the all different bending-stretching situation.

https://dx.doi.org/10.22161/ijaers.74.18 ISSN: 2349-6495(P) | 2456-1908(O)

Meanwhile, the practical experiment indicates that the aspheric-shape ZIF-8 can mobilize in-line with the flexible substrate SSWM, without disintegrating effect on the electrode surface. Moreover, the less conductance of C-ZIF-8, solved by electrodeposition the conductive polymer PANI on the seed layer C-ZIF-8, by preforming unipolar pulse electroception method (UPED), mainly during the on-time and flowing of current-voltage of 0.8V, PANI monomer electrodeposit from the electrolyte (1M H_2SO_4, 0.5M PANI) to the electrode surface, and during the relaxation off-time without flowing current, PANI chain permeates inside the aspheric-shape C-ZIF-8 intrinsic aggregation matrix, creating a pathway for the electrons, concomitantly increasing the conductance of the electrode matrix.

UPED strategy with adjustment for the electrodeposition cycles and time is a significant factor in the result mentioned above. Controlling the electrodeposition time and cycles, led to incase or covered all aspheric-shape C-ZIF-8 particles in individual scale, due to relatively long relaxation time (off-time), furthermore enhancement the particles coherency in the electrode matrix, due to the epoxy properties for the conductive polymer PANI. Herein as such electrode materials accumulate the features of high surface area, excellent conductance, the electrode material can mobilize compatible with the flexible substrate with unique capability of losing the flexion strength by converging or diverging the aspheric-shape particles (C-ZIF-8). However, the electrode thickness is significant factor on the flexible supercapacitor devise, and it must be determined and specified, because thick electrode layer could easily affect by the flexion strength, which led to collapse or fragmentizes the electrode surface.

It worth to noting that PANI can electrodeposited in different morphologies (nanorods, nanofibers, or arrays) on various substrates, precisely the nanorods morphology could shorten the electron pathway. Moreover, the emptiness between the nanorods could relatively gain more surface area in the electrode, to accommodate the storage electrons, induced by electrochemical reactions (charge-discharge process) [10-12], and the magnificent structure of PANI nanorods growth on the top of aspheric-shapes C-ZIF-8 particles seed layer, capable to reeling the active electrode materials compatibly with the flexible substrate, rustling in withstanding the electrode surface under critical flexions degree. Moreover, PANI nanorods growth on low current density, which means electrodeposit PANI layer, would gain thinner thickness, due to conversion a few amounts of PANI monomer from the electrolyte to PANI chain on/or inside the C-ZIF-8 seed layer, meanwhile conserve the influence of the aspheric C-ZIF-8 seed layer, simultaneously avoid backfill it by thick PANI layer, which can preserve the mechanical mechanism of the aspheric-shape particles C-ZIF8 (converge or diverge). Therefore, monitoring the electrodeposit process and adjust the electrodeposition cycles, time and thickness could be efficiency done by UPED method [13], precisely by prepare different sample, with ascending increase the electrodeposit amount of PANI, follow by pursuit the electrodeposition surface morphology in each sample, to determine the starting-point of the nanorods growth.

Herein PANI nanorods grow in the aspheric C-ZIF-8 seed layer by preforming unipolar pluse electrodeposition strategy (UPED), the electrochemical circuit built-in stainless steel warmish (SSWM), the fabricating of the ultra-thin electrode layer, and the growing of PANI nanorod investigate and determined by prepared six sample with vary-in the electrodeposit cycles of PANI, the samples named according to the electrodeposit PANI cycles, in such a way 05 UPED cycles, 10 UPED cycles, 15 UPED cycles, 20 UPED cycles, 25 UPED cycles, and 50 UPED cycles. The morphology of the electrode surface characterization investigates by SEM, XRD, FTIR and BET surface measurement to understand and pursue the growth of PANI nanorods, at the lowest possible thickness, beside the role of UPED strategy has been discussed.

II. EXPERIMENTAL

2.1. Materials

Polyaniline (PANI), 2-methyl-imidazole Zn $(NO_3)_2{\cdot}6H_2O$, polyvinylidene fluoride alcohol (PVDF), conductive carbon, polyvinyl alcohol (molecular weight of 98000 $g{\cdot}mol^{-1}$), H_2SO_4 (98%), N-methylpyrolidone (C_5H_9NO) solutions, were provided from Shanghai Chemicals, Co. Ltd. China. Flexible substrate SSWM with a pore diameter of 40 μm (400 mesh) was purchased from Hardware-Product, HeBei Co. Ltd. China. The SSWM was cut to a size of 2 × 2 cm^2, and polished with sandpaper, further treated with ultrasound in aqueous ethanol for 15 minutes, and dried in oven 50 °C for 12 h. sticky tape carefully covered one side of the SSWM for mathematical calculation purposes. Millipore water (18.2 MΩ cm) was used to prepare all the solutions.

2.2. Preparation of aspheric-shape ZIF-8.

The preparation process for aspheric-shape C-ZIF-8 partials done according to the reference [14], (0.183 g of $Zn(NO_3)_2{\cdot}6H_2O$, 0.405 g of 2-methylimidazole) was dissolved in (6, 10 mL) of methanol respectively, and the two solutions firstly were stirred individual for an hour. Then mixed and stirred for 0.5 hour. After that, Teflon-lined

https://dx.doi.org/10.22161/ijaers.74.18 ISSN: 2349-6495(P) | 2456-1908(O)

autoclave contains the solution heated at 110 °C overnight. The white precipitation collected by centrifugation (10000 rpm for 20 min) and washed carefully with methanol. At last ZIF -8 was carbonized at 900 °C for 6 hours under an argon atmosphere. C-ZIF-8 further rinse with ethanol/water several times and dried overnight [15].

2.3. Preparation of C-ZIF-8 seed layer on the flexible substrate electrode

C-ZIF-8, polyvinylidene fluoride alcohol (PVDF), conductive carbons, mixed according to the percentage of 8:1:1 respectively, the powder further mixed with N-methylpyrolidone (C_5H_9NO) solutions under stirring overnight, the obtained ink was used to coat the pre-treated SSWM. Finally, the electrode C-ZIF-8/SSWM sample obtained and dried overnight [16].

2.4. Electrodeposition PANI on the C-ZIF-8 seed layer by UPED method

UPED method performed in three-electrode configuration, C-ZIF-8/SSWM, saturated calomel electrode (SCE) and Pt sheet used as working electrode, reference and counter electrode respectively. All the electrochemical cell immersed in 1M sulfuric acid and 0.5 M aniline, and the electrodeposition was done at room temperature. The current-voltage set at 0.8 V with 5.0 s off-time (t-off) and 0.5 s on-time (t-off) [13]. Each of the different sample prepared by electrodeposited 5 consecutive UPED cycles on the aspheric-shape C-ZIF-8 seed layer, small piece toke from the first sample for more investigation. The second sample prepared by continues electrodeposit 5 consecutive UPED cycles in the same electrode surface and cutting a small piece for surface investigation, the same procedures repeat for the all prepared sample.

2.5. Electrochemical characterization

The carbonization process for the aspheric-shape ZIF-8 investigates by BET surface measurement. Also, the growth of PANI on the C-ZIF-8 seed layer investigates and monitor by (SEM, X-RD and FTIR spectroscopy). All the preparation steps are done in the normal room temperature. Princeton, (VMP3) adjusted with EC-Lab software used to conduct the experiment.

III. RESULTS AND DISCUSSION

3.1. Structural and morphology characterization

Fig. 1(A-B) shown the seed layer C-ZIF-8 particles, successfully syntheses by our prementioned method, the surface morphology of C-ZIF-8 is polyhedron high surface area, construct from individual deformed aspheric particles shape, the irregular multi-face shape capable of converging or diverging in-line compatibly with flexible substrate SSWM, without any side effect on the electrode surface. Fig. 1(C-D) show the C-ZIF-8 after the carbonization process at 900 ºC in the Ar atmosphere, all the particles tend to be bord and rougher, due to carbonize the organic linker, which directly enhances the general circuit conductance, Moreover, the thorough coating of the C-ZIF-8 seed layer on the flexible substrate, successfully backfill the voids on the SSWM substrate. Fig. 2(A-B) shown the preparation of the first sample 5 UPED cycles, one can see the PANI chain penetrate inside the seed layer matrix, due to the gaps between the aspheric-shape particles, the result gives the evidence that the electrodeposit amount of PANI is low, and not enough to incase or cover the aspheric-shapes particles. Fig. 2(C-D) shown the sample of 10 UPED cycles, PANI electrodeposits on the C-ZIF-8 seed layer by 10 consecutive UPED cycles. The particle domain tends to be relatively hemogenic, but still the majority of the aspheric-shapes particles is naked. Fig. 3(A-B) shown the sample of 15 UPED cycles, PANI electrodeposit on the C-ZIF-8 seed layer by 15 consecutive UPED cycles, the surface morphology appeared relatively homogeneous, and most of the aspheric-shapes particles tend to be encased or covered by PANI chain, but still non-PANI nanorod formed yet. Fig. 3(C-D) shown the sample of 20 UPED cycles, PANI electrodeposits on the C-ZIF-8 seed layer by 20 consecutive UPED cycles, herein clearly can see the whole C-ZIF-8 seed layer covered by PANI nanorod. As a result, enhancing the cohesion in the whole circuit, the morphology of transformation PANI from aspheric-shape to cylindrical shape, attribute to the anilinium micellar transformed from the electrolyte to the seed layer surface, in the existence of current (on-time) and the acidic environment (H_2SO_4), also the polymer chain interaction backbone after each on-off electrodeposit cycle, drive the PANI to grow into nanorod morphology [17-18], consensus result has been reported by Jang J and his Co-worker [19]. Besides, the emptiness between the nanorods create an additional pathway and active area to storage the electrons, more importantly, the thickness of the C-ZIF-8/PANI is (10-20 µm), as such thickness allow the whole circuit mobilize compatibly in-line with SSWM when the flexible device exposed to manipulating or flexion strength. Fig. 4(A-B) shown the sample of 25 UPED cycles, PANI electrodeposit on the C-ZIF-8 seed layer by 25 consecutive UPED cycles, the surface morphology deliver the avoidances of the PANI electrodeposit chain backfill the domain between the particles, and exceed that to pile the whole matrix by thick overlapping PANI chain layer, besides that less PANI nanorod formation observe, This new outcomes of thick PANI layer, could hinder the convergence or divergence

https://dx.doi.org/10.22161/ijaers.74.18 *ISSN: 2349-6495(P) | 2456-1908(O)*

between C-ZIF-8 seed layers, in-word electrodeposit more than 20 consecutive UPED cycles could threaten the electrode flexibility. Fig. 4(C-D) shown the sample of 50 UPED cycles, PANI electrodeposit on the C-ZIF-8 seed layer by 50 consecutive UPED cycles, the experiment performed to investigate the surface characteristic after electrodeposit thick PANI layer, the surface morphology tends to be more hemogenic, with an absence of PANI nanorod formation.

3.2 XRD Diffraction

Fig. 5 shows X-ray diffraction (XRD) of ZIF-8, C-ZIF-8, and C-ZIF-8/PANI. The characteristic diffraction patterns of C-ZIF-8 disappear due to the carbonization, and only two broad patterns at $2\theta = 25°$ and 44° exist after the carbonization, revealing the successful conversion from C-ZIF-8 to carbon materials. The border peaks of C-ZIF-8 are identical signals of amorphous carbon [20], no diffraction peaks of the impurity can be observed. C-ZIF-8/PANI exhibits diffraction peak at vicinity $2\theta = 10°$ to 20°, and it can be assigned to the crystalline PANI [21]. However, the diffraction peak at 44° is symmetrical to the amorphous carbon, confirming and reveal the successful electrodeposition of the PANI in the C-ZIF-8 surface.

3.3 FTIR Spectra Scopey

Fig. 6 shows the FTIR spectra of the C-ZIF-8, C-ZIF-8, and C-ZIF-8/PANI. As can be observed, C-ZIF-8 show two peaks located at 3300 and 2827 cm^{-1}, corresponding to the aromatic and aliphatic C–H and N-H stretching band of imidazole (the organic linker), respectively [22]. It realizable that these peaks remind without a noticeable change in the following preparation process, which is strong evidence to the residual of the shape of the aspherical particles even after the carbonization [23], The peak at 1610 cm^{-1} is ascribed to C=N stretching, while the bands in the spectral region of 400 – 1500 cm^{-1} are associated with the stretching or bending of the entire ring, these peaks are identical with those of a previous report [24]. C-ZIF-8 spectral shown absence for the most of ZIF-8 peaks after the carbonization, a broad absorption band recorded around 3300 cm^{-1}, attributable to C–H and O–H stretching vibrations, as well as other characteristic peaks around 1610 and 1290 cm^{-1} corresponding to carbon band C≡N and C–N respectively [25]. C-ZIF-8/PANI nanorod exhibit a border peak at 3300 cm^{-1}, assigned to C–H stretching vibration derived from the imidazole as it prementioned, two distinct bands at 2820 and 1643 cm^{-1} which are attributed to the asymmetrical carbon stretching vibration of C–H and the O–H respectively [26], The absorption bands at 1556 and 1390 cm^{-1} in the spectrum of PANI can be assigned to the stretching vibrations of the quinoid (N=Q=N) and benzoin (N–B–N) structure respectively [27]. This stacking interaction of the peaks during different syntheses process demonstrates the successful preparation of the composite PANI nanorod on the C-ZIF-8 surface.

Fig. 7 shows BET surface measurement for ZIF-8 and C-ZIF-8. Fig. 3(A) is indicating that the surface contains mesopore and microporous particles. derive from ZIF-8, [28]. Nevertheless, the carbonization at 900C resulting in decrease surface area from (1701 nm^2) to (1200 nm^2) [29]. Fig. 3(B) shown C-ZIF-8 and C-ZIF-8 BET surface measurement and pore size distribution. Therefore, the heat treatment of ZIF-8 resulted in the modification the pore size distribution, and this feature, along with the high polyhedron surface area, facilitates the diffusion of electrons into the carbon network and helps to increase the adsorption capacity of the materials. The effect of heat treatment on the surface area of ZIF-8 is inconsistent with the results reported by Gadipelli et al. [30], in their study, it was shown that carbonized MOF-5 (containing Zn) at temperatures below 900 °C resulted in a decrease in surface area. On the contrary, heat treatment at temperatures higher than the evaporation temperature of Zn (908 °C) caused an increase in the surface area. The reason attributed to the reduction of ZnO with carbon and the evolution of Zn, CO, and CO2, which results in more porous network.

3.4 UPED Electrodeposition

Fig. 8 demonstrate the efficiency electrodeposition method UPED, herein the continuous decline on the peaks after each 5 consecutive cycles, attributed to the drop in the aniline concentration from the electrolyte after fabrication each sample, the first fabricated sample (05 UPED cycles) record the higher peaks, due to the higher concentration of the aniline. Also, the general circuit resistance is low, due to the excellent conductance of the aniline in the binging of the reaction. Descending peaks recorded in the flowing fabricating sample 10,15, and 20 UPED cycles, respectively, mainly due to the gradual decline in the concentration of the PANI in the electrolyte after any sample fabrication. As a result of the decreasing in the concentration of PANI from the electrolyte, face increasing in fabricated sample mass wight, as such evidence present the efficiency of UPED method and capability to monitoring the thickness of the fabricated sample.

IV. FIGURES AND TABLES

https://dx.doi.org/10.22161/ijaers.74.18 *ISSN: 2349-6495(P) | 2456-1908(O)*

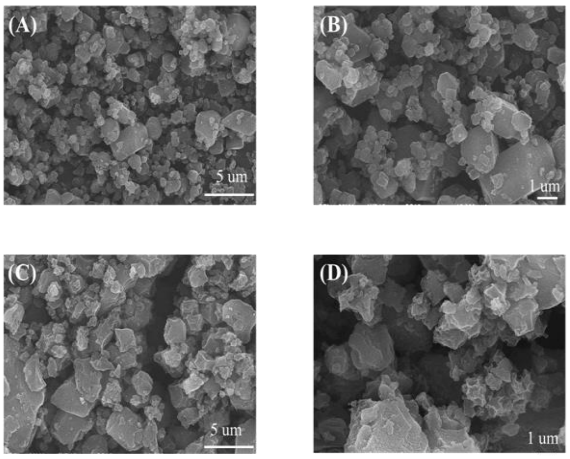

Fig. 1 SEM characterization (A-B) as Syntheses ZIF-8, (C-D) C-ZIF-8 after the carbonization process.

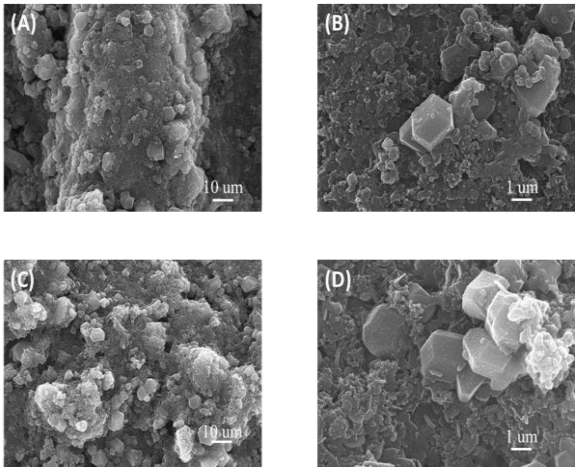

Fig. 2 SEM characterization of C-ZIF-8/PANI, (A-B) after electrodeposit 05 UPED cycles to Syntheses C-ZIF-8/PANI, (C-D) after electrodeposit 10 UPED cycles to Syntheses C-ZIF-8/PANI.

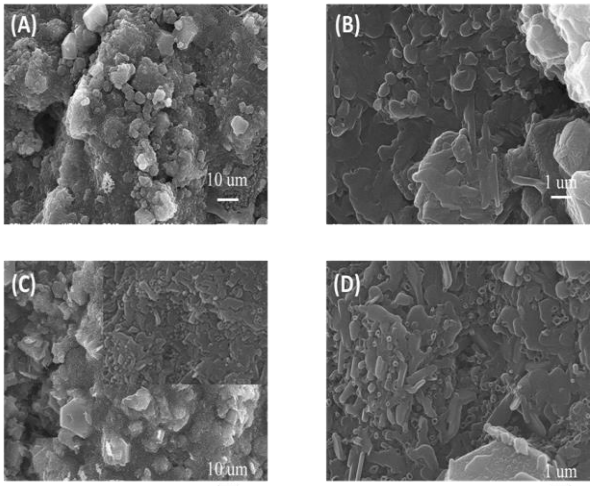

Fig. 3 SEM characterization of C-ZIF-8/PANI, (A-B) after electrodeposit 15 UPED cycles to Syntheses C-ZIF-8/PANI, (C-D) after electrodeposit 20 UPED cycles to Syntheses C-ZIF-8/PANI.

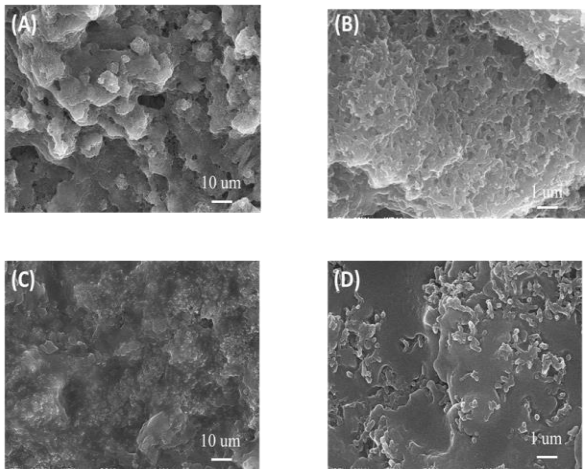

Fig. 4 SEM characterization of C-ZIF-8/PANI, (A-B) after electrodeposit 25 UPED cycles to Syntheses C-ZIF-8/PANI, (C-D) after electrodeposit 50 UPED cycles to Syntheses C-ZIF-8/PANI.

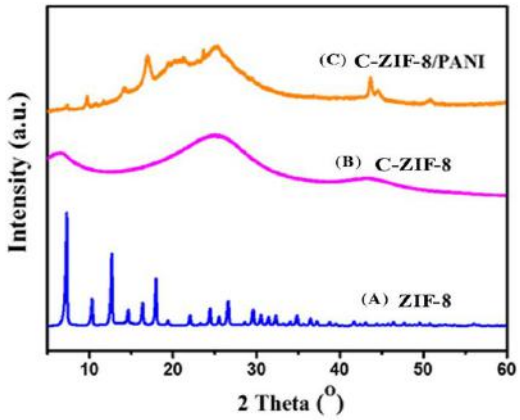

Fig. 5 X-ray diffraction (XRD) of ZIF-8, C-ZIF-8, and C-ZIF-8/PANI.

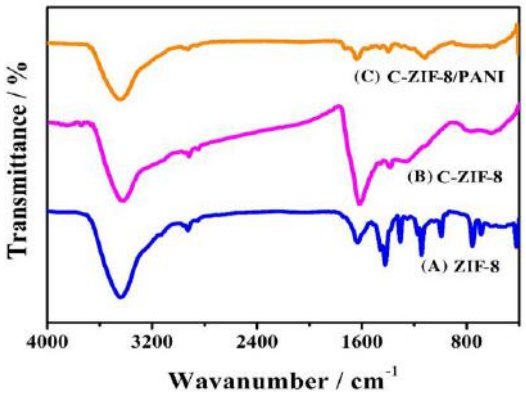

Fig. 6 FTIR spectra of the ZIF-8, C-ZIF-8, and C-ZIF-8/PANI.

https://dx.doi.org/10.22161/ijaers.74.18 *ISSN: 2349-6495(P) | 2456-1908(O)*

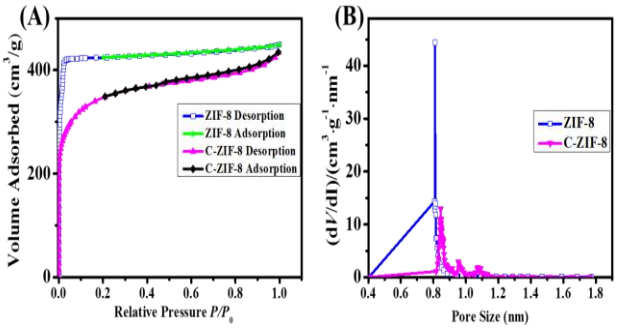

Fig. 7 shown A-B, ZIF and C-ZIF-8 BET surface measurement, pore size distribution respectively.

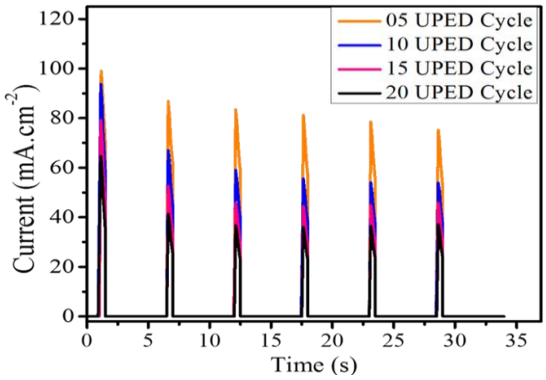

Fig. 8 UPED electrodeposition method with current voltage of 0.8V and 0.5,5.0 s on-off time respectively.

V. CONCLUSION

In summary, we have developed a Preparation protocol of PANI nanorods grow on the C-ZIF-8 seed layer by preforming UPED electrodeposition method, as Ultra-thin elastic electrode for the flexible capacitor. UPED electrodeposition method allows to customizing the growth of PANI nanorods on aspheric-shape C-ZIF-8 within the thickness of (10-20 µm), by controlling the transformation of the anilinium micellar, and the interaction in the polymer chain backbone, through controlling the open circuit electrodeposition cycles and time. The comparison of the different produced samples delivers the evidence that at 20 UPED cycles PANI grew in nanorod formation, the unique structure endows the whole electrode matrix a mechanical elasticity to move in-line with the flexible substrate. The method presented here is suitable for the development of ultra-thin flexible electrode materials, this will provide a new opportunity for enriching relevant MOF-based electrode materials in flexible energy conversion and storage devices.

ACKNOWLEDGEMENTS

This work is supported by the National Natural Science Foundation of China (21776191, 21706181) and the International Science & Technology Cooperation Program of China (No. 2017YFE0129200) and the International Science & Technology Cooperation Program of Shanxi Province (No. 201803D421094).

REFERENCES

[1] Yang Y, Zhang Y, Zhu C, Xie Y, Lv L, Chen W, Hu Z (2020). Synthesis of ultrafine CoNi2S4 nanowire on carbon cloth as an efficient positive electrode material for high-performance hybrid supercapacitors. Journal of Alloys and Compounds, 823, 153885.https ://doi.org/10.1016/j.jallcom.2020.153885.

[2] Zheng Y, Yang Y, Chen S, Yuan Q (2016). Smart stretchable and wearable supercapacitors: prospects and challenges. Journal of Crystal Engineering Community, 18(23), 4218-4235.https://doi.org/10.1039/C5CE02510A.

[3] Wang C, Kaneti Y, Bando Y, Lin J, Liu C, Li J, Yamauchi Y (2018). Metal–organic framework-derived one-dimensional porous or hollow carbon-based nanofibers for energy storage and conversion. Materials Horizons, 5(3), 394-407.https://doi.org/10.1039/C8MH00133B.

[4] Pu J, Wang X, Xu R, Xu S, Komvopoulos K (2018). Highly flexible foldable and rollable microsupercapacitors on an ultrathin polyimide substrate with high power density. Microsystems & nanoengineering, 4(1), 1-11. https:// doi.org/10.1038/s41378-018-0016-3.

[5] Wang K, Zhao P, Zhou X, Wu H, Wei Z (2011). Flexible supercapacitors based on cloth-supported electrodes of conducting polymer nanowire array/SWCNT composites. Journal of Materials Chemistry, 21(41), 16373-16378. https://doi.org/10.1039/C1JM13722K.

[6] Liu Y, Narayanasamy M, Yang C, Shi M, Xie W, Wu H, Guo Z (2019). High-performance coaxial wire-shaped supercapacitors using ionogel electrolyte toward sustainable energy system. Journal of Materials Research, 34(17), 3030-3039. https://doi.org/10.1557/jmr.2019.234.

[7] Fu X. Y, Chen Z, Zhang Y, Han D, Ma, Wang W, Sun H (2019). Direct laser writing of flexible planar supercapacitors based on GO and black phosphorus quantum dot nanocomposites. Nanoscale, 11(18), 9133-9140. https://doi.org/10.1039/C9NR02530H.

[8] Areir M, Xu Y, Harrison D, Fyson J (2017). 3D printing of highly flexible supercapacitor designed for wearable energy storage. Materials Science and Engineering: B, 226, 29-38.https://doi.org/10.1016/j.mseb.2017.09.004.

[9] Yanilmaz M, Dirican M, Asiri A, Zhang X (2019). Flexible polyaniline-carbon nanofiber supercapacitor electrodes. Journal of Energy Storage, 24, 100766. https://doi.org/10.1016/j.est.2019.100766.

[10] Xiong G, Meng C, Reifenberger R, Irazoqui P, Fisher T (2014). graphitic petal electrodes for all-solid-state flexible

supercapacitors. Advanced Energy Materials, 4(3), 1300515.https://doi.org/10.1002/aenm.201300515.

[11] Gaikwad A, Arias A (2017). Understanding the effects of electrode formulation on the mechanical strength of composite electrodes for flexible batteries. ACS applied materials & interfaces, 9(7) 6390-6400. https://doi.org/10.1021/acsami.6b14719.

[12] Choi C, Kim K, Kim J, Lepró X, Spinks G, Baughman R, Kim S (2016). Improvement of system capacitance via weavable superelastic biscrolled yarn supercapacitors. Nature communications, 7(1), 1-8. https://doi.org/10.1038/ncomms13811.

[13] Du X, Zhang H, Hao X, Guan G, Abudula A (2014). Facile preparation of ion-imprinted composite film for selective electrochemical removal of nickel (II) ions. ACS applied materials & interfaces, 6(12), 9543-9549. https://doi.org/10.1021/am501926u.

[14] Zhang H, Hou J, Hu Y, Wang P, Ou R, Jiang L, Wang H (2018). Ultrafast selective transport of alkali metal ions in metal organic frameworks with subnanometer pores. Science Advances, 4(2), eaaq0066. https://doi.org/10.1126/sciadv.aaq0066.

[15] Zhang J, Yan X, Hu X, Feng R, Zhou M (2018). Direct carbonization of Zn/Co zeolitic imidazolate frameworks for efficient adsorption of Rhodamine B. Chemical Engineering Journal, 347, 640-647. https://doi.org/10.1016/j.cej.2018.04.132.

[16] Wang P, Du X, An X, Li S, Gao F, Hao X, Guan G (2017). Synthesis of oriented coral-like polyaniline nano-arrays for flexible all-solid-state supercapacitor. Synthetic Metals, 232, 87-95. https://doi.org/10.1016/j.synthmet.2017.07.023.

[17] Yang J, Ding Y, Chen G, Li C (2007). Synthesis of conducting polyaniline using novel anionic Gemini surfactant as micellar stabilizer. European Polymer Journal, 43(8), 3337-3343. https://doi.org/10.1016/j.eurpolymj.2007.04.040.

[18] Wang Z, Hao X, Zhang Z, Liu S, Liang Z, Guan G (2012). One-step unipolar pulse electrodeposition of nickel hexacyanoferrate/chitosan/carbon nanotubes film and its application in hydrogen peroxide sensor. Sensors and Actuators B: Chemical, 162(1), 353-360. https://doi.org/10.1016/j.snb.2011.12.099.

[19] Jang J, Bae J, Lee K (2005). Synthesis and characterization of polyaniline nanorods as curing agent and nanofiller for epoxy matrix composite. Polymer, 46(11), 3677-3684. https://doi.org/10.1016/j.polymer.2005.03.030.

[20] Yu H, Zhu W, Zhou H, Liu J, Yang Z, Hu X, Yuan A (2019). Porous carbon derived from metal–organic framework@ graphene quantum dots as electrode materials for supercapacitors and lithium-ion batteries. Royal Society of Chemistry Advances, 9(17), 9577-9583. https://doi.org/10.1039/C9RA01488H.

[21] Eskizeybek V, Sarı F, Gülce H, Gülce A, Avcı A (2012). Preparation of the new polyaniline/ZnO nanocomposite and its photocatalytic activity for degradation of methylene blue and malachite green dyes under UV and natural sun lights irradiations. Applied Catalysis B: Environmental, 119, 197-206.https://doi.org/10.1016/j.apcatb.2012.02.034.

[22] Cai C, Zou Y, Xiang C, Chu H, Qiu S, Sui Q, Shah A (2018). Broccoli-like porous carbon nitride from ZIF-8 and melamine for high performance supercapacitors. Applied Surface Science, 440, 47-54. https://doi.org/10.1016/j.apsusc.2017.12.242.

[23] Wang S, Cui J, Zhang S, Xie X, Xia W (2020). Enhancement thermal stability and CO2 adsorption property of ZIF-8 by pre-modification with polyaniline. Materials Research Express, 7(2), 025304. https://doi.org/10.1088/2053-1591/ab6db3.

[24] Jiang M, Cao X, Zhu D, Duan, Y, Zhang J (2016). Hierarchically porous N-doped carbon derived from ZIF-8 nanocomposites for electrochemical applications. Electrochimica Acta, 196, 699-707. https://doi.org/10.1016/j.electacta.2016.02.094.

[25] Yanilmaz M, Dirican M, Asiri A M, Zhang X. (2019). Flexible polyaniline-carbon nanofiber supercapacitor electrodes. Journal of Energy Storage, 24, 100766. https://doi.org/10.1016/j.est.2019.100766.

[26] Cai C, Zou Y, Xiang C, Chu H, Qiu S, Sui Q, Shah A (2018). Broccoli-like porous carbon nitride from ZIF-8 and melamine for high performance supercapacitors. Applied Surface Science, 440, 47-54. https://doi.org/10.1016/j.apsusc.2017.12.242.

[27] Hu X, Ou Y, Liu G, Gao M, Song L, Zang J, Chen W (2018). Synthesis and characterization of the conducting polymer micro-helix based on the Spirulina template. Polymers, 10(8), 882. https://doi.org/10.1016/j.apsusc.2017.12.242.

[28] Abbasi Z, Shamsaei E, Leong S, Ladewig B, Zhang X, Wang H (2016). Effect of carbonization temperature on adsorption property of ZIF-8 derived nanoporous carbon for water treatment. Microporous and Mesoporous Materials, 236, 28-37. https://doi.org/10.1016/j.micromeso.2016.08.022.

[29] Pan Y, Liu Y, Zeng G, Zhao L, Lai Z (2011). Rapid synthesis of zeolitic imidazolate framework-8 (ZIF-8) nanocrystals in an aqueous system. Chemical Communications, 47(7), 2071-2073. https://doi.org/10.1016/j.micromeso.2016.08.022.

[30] Srinivas G, Krungleviciute V, Guo Z, Yildirim T (2014). Exceptional CO2 capture in a hierarchically porous carbon with simultaneous high surface area and pore volume. Energy & Environmental Science, 7(1), 335-342. https://doi.org/10.1039/C3EE42918K.